Available online at www.sciencedirect.com
SCIENCE DIRECT®
Applied Thermal Engineering 24 (2004) 717–733
APPLIED THERMAL ENGINEERING
www.elsevier.com/locate/apthermeng

Thermal applicability of two-phase thermosyphons in cooking chambers—experimental and theoretical analysis

A.K. da Silva *, M.B.H. Mantelli

Satellite Thermal Control Group, Department of Mechanical Engineering, Federal University of Santa Catarina, P.O. Box 476, Florianópolis, SC 88040-900, Brazil

Received 9 June 2003; accepted 30 September 2003

Abstract

This paper studies the thermal applicability of two-phase thermosyphons in ovens/furnaces. The objective is to evaluate the performance of thermosyphons as heat transfer devices responsible for connecting the combustion and cooking chambers. Two different approaches were used: first, an experimental setup, which simulates an internal cross section of a convectional bakery oven cooking chamber assisted by vertical thermosyphons, was built. The experimental measurements show that the thermosyphons were able to provide a uniform temperature distribution inside the cooking chamber without the appearance of any overheated spot. In addition to the experimental setup, a theoretical lumped model was used to predict the air temperature variation and the relative importance of the convective and radiative heat transfer modes inside the cooking chamber. The net radiation heat transfer between the internal walls was determined numerically by means of a method described in [20]. The finite difference technique was applied for the computation of the non-linear differential system. The comparison between the model and the experimental data can be considered good, and the radiation was the major heat transfer mechanism inside the cooking chamber.

Keywords: Convection; Radiation; Thermosyphon; Cooking chamber

* Corresponding author. Present address: Department of Mechanical Engineering and Materials Science, Duke University, P.O. Box 90300, Durham, NC 27708-0300, USA. Tel.: +1-919-660-5299; fax: +1-919-660-8963.
E-mail address: akd3@duke.edu (A.K. da Silva).

1359-4311/$ - see front matter
doi:10.1016/j.applthermaleng.2003.09.013

Nomenclature

A	area, m^2
b	thickness, m
C	global conductance, $W\,m^{-1}\,K^{-1}$
c_p	specific heat, $J\,kg^{-1}\,K^{-1}$
F	view factor
g	gravity, $m\,s^{-2}$
G	yield radiation coefficient
h	heat transfer coefficient, $W\,m^{-2}\,K^{-1}$
H	height, m
I	current, A
k	thermal conductivity, $W\,m^{-1}\,K^{-1}$
L	length, m
$\overline{Nu}_L$	average Nusselt number
P	experimental power applied, W
q'	heat flux, $W\,m^{-1}$
$\hat{q}$	dimensionless heat flux
Q	heat transfer rate, W
Pr	Prandtl number
Re	Reynolds number
t	time, s
$\hat{t}$	dimensionless time
T	temperature, °C
$\overline{T}$	average temperature, °C
U	overall heat transfer coefficient, $W\,m^{-2}\,K^{-1}$
v	characteristic velocity, $m\,s^{-1}$
V	volume, m^3, voltage, V
x, y, z	Cartesian coordinates, m

Greek symbols

α	absorptivity, thermal difussivity, $m^2\,s^{-1}$
ε	emissivity
v	kinematic viscosity, $m^2\,s^{-1}$
ρ	reflectivity
σ	Stefan–Boltzmann constant, $W\,m^{-2}\,K^{-4}$

Subscripts

1, 2, 3, 4	internal surfaces index
air	enclosed air
avg, e	average external
avg, i	average internal
e	evaporator

c	condenser
conv	convective
film	film temperature
$i, j, \ldots, N$	surface general index
I	insulation
L	characteristic length
ms	metal sheet
out	outside the cooking chamber
rad	radiative

1. Introduction

Energy generation and conservation has received special attention all over the world. This is the main concern of several industries that are forced to save energy and reduce the production costs [1]. Good examples are the companies that produce electric bakery ovens, since the energy consumption in such devices is an important issue, especially for small business. Besides this economic factor, which can be related to performance, functionality is also a major issue. The thermal characteristics of the actual ovens do not provide a uniform temperature distribution inside the cooking chamber. Usually these ovens have an electrical resistance located inside the cooking chamber. The resistance (i.e., heat source) has a small heat transfer area when compared with the volume to be heated, which creates over-heated regions. Spreading out the heat sources inside the oven's cooking chamber can easily solve this problem, although it is too expensive.

As an alternative solution, big blowers are installed inside the cooking chamber in order to turn the temperature uniform. However, big electric motors consume lots of energy itself, and in spite of that it is known that radiation is the major heat transfer mechanism inside enclosures [2–9]. Carvalho and Martins [10] performed a very specific numerical study considering a three-dimensional turbulent flow of air and steam inside a cooking chamber, emphasizing the heat and mass transfer modes. They stressed the importance of the radiative heat flux as a major mechanism, showing that the radiation represents more than 70% of the total energy absorbed by the bread dough inside the oven at a cooking temperature equal to 200 °C. Based on that we can conclude that the ideal situation is the one in which the heat sources inside the cooking chamber have large areas and temperatures slightly greater than the ideal cooking temperature. Based on such conclusion, how can we come up with a solution thermally and economically viable?

To answer this question, the Satellite Thermal Control Group (NCTS) is studying the use of two-phase thermosyphons in ovens working as a heat transfer device, which connects thermally the combustion and cooking chambers. Several studies have been reported demonstrating the successful applicability of thermosyphons in other applications [11–16]. However, for the first time, vertical thermosyphons with an unusual geometry (i.e., thermosyphons where the condenser is five times larger than the evaporator in length) have been used in ovens. A preliminary study by Mantelli et al. [17] showed that the new geometric configuration used in the present study, which is required to a thermosyphon to "fit" inside a convectional oven, presents a good thermal performance.

In the present work, we proposed to investigate the behavior of thermosyphons exposed to real conditions in cooking chambers. For that, an experimental prototype, which simulates the cross section of the commercial oven, was built. Four vertical thermosyphons were installed inside the prototype. The experimental measurements were compared with the results generated by a theoretical lumped model, which takes into account the convective and radiative effects inside the cooking chamber.

2. Theoretical model

In the present model, a transient heat transfer balance between the internal surfaces of a cooking chamber and the enclosed air is performed. The physical model described in Fig. 1 is based on the experimental setup built by NCTS, later in this study. The interaction among the four internal walls is taken into account. The enclosure is filled with air, which is considered a non-participating gas in the radiation net. The radiation scattering is neglected and the forced convection flow in the internal walls is considered well mixed. The relative influence of the wall radiation properties and the forced convection, represented by the Reynolds number ($Re = vL/v$), are examined, where v represents a characteristic velocity (i.e., the mean flow velocity over a referred plate), L is the characteristic length of the plate and v is the kinematic viscosity.

This model consists of the heat transfer balance among the air inside the cooking chamber, the top and bottom horizontal surfaces, and two vertical lateral surfaces. The air temperature was named T_{air}, and the temperature of the top and bottom surfaces were named T_2 and T_4 respectively. The vertical walls surfaces temperatures, T_1 and T_3, are considered equal and prescribed, varying according to the experimental data, described later in this study. The conduction heat transfer between the internal walls and the heat losses between the vertical walls and the exterior environment are neglected. On the other hand, heat transfer between the horizontal walls and the outside environment is considered. The overall heat transfer coefficients between the horizontal

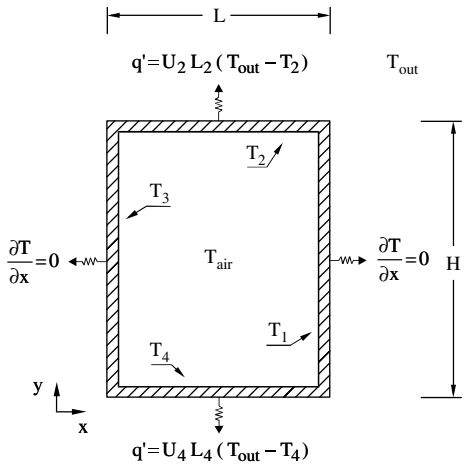

Fig. 1. Theoretical physical model for the enclosure with transient temperatures.

walls and the environment were named U_2 and U_4. They are concerned with the top and bottom walls respectively.

The transient heat exchange between the walls and the air happens through convection, while the transient heat transfer between the internal walls is through convection and radiation. The heat balance for the enclosed air is given by

$$\rho_{\text{air}} c_{p,\text{air}} V_{\text{air}} \frac{\mathrm{d}T_{\text{air}}}{\mathrm{d}t} = 2h_1 A_1 [T_1 - T_{\text{air}}] + h_2 A_2 [T_2 - T_{\text{air}}] + h_4 A_4 [T_4 - T_{\text{air}}] \tag{1}$$

In the above equation, the three right hand side terms represent the energy obtained by forced convection from the surfaces 1, 2 and 4 respectively. The convective heat transfer coefficients between the walls and the air, h_1, h_2 and h_4, are functions of the respective wall's temperature, and were calculated according to the film temperature of each surface. For surfaces 1 and 3, the film temperature is defined as $T_{\text{film},1} = (T_1 - T_{\text{air}})/2$, for surface 2, $T_{\text{film},2} = (T_2 - T_{\text{air}})/2$, and finally for surface 4, $T_{\text{film},4} = (T_4 - T_{\text{air}})/2$. A_1, A_2 and A_4, are the internal surface areas for the vertical, top and bottom walls respectively. The three left hand side parameters ($\rho_{\text{air}}, c_{p,\text{air}}$ and V_{air}) are the density, the specific heat and the volume of the air inside the enclosure.

Another balance given by Eq. (2), evaluates the temperature variation of surface 2 considering three effects. On the right hand side, the first term represents the convective heat transfer between this surface and the inside air, the second term determines the heat losses to the outside environment, and the third term represents the liquid radiation heat flux reaching this surface. A similar energy balance is obtained for surface 4, and it is given by Eq. (3), where the same three terms described for Eq. (2) can be found. Eqs. (1)–(3) form a non-linear and non-homogeneous system of differential equations.

$$\rho_2 c_{P,2} V_2 \frac{\mathrm{d}T_2}{\mathrm{d}t} = h_2 A_2 (T_{\text{air}} - T_2) + U_2 A_2 (T_{\text{out}} - T_2) + \sum_{i=1}^{4} A_2 \varepsilon_2 \sigma G_{2-i} \left(T_i^4 - T_2^4\right) \tag{2}$$

$$\rho_4 c_{P,4} V_4 \frac{\mathrm{d}T_4}{\mathrm{d}t} = h_4 A_4 (T_{\text{air}} - T_4) + U_4 A_4 (T_{\text{out}} - T_4) + \sum_{i=1}^{4} A_4 \varepsilon_4 \sigma G_{4-i} \left(T_i^4 - T_4^4\right) \tag{3}$$

In Eqs. (2) and (3), the two overall coefficients, U_2 and U_4, take into account the heat transfer through the internal metal sheet, the prototype insulation layer, the external metal sheet and the outside convection heat transfer. Figure 2 gives a detailed view of the top surface. These overall coefficients are defined in Eqs. (4) and (5):

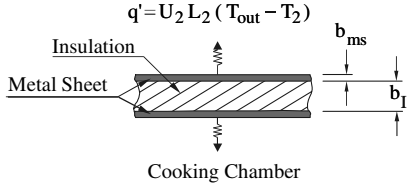

Fig. 2. Top surface insulation detail.

$$U_2 = \left[2\left(\frac{b_{ms}}{k_{ms}}\right) + \left(\frac{b_I}{k_I}\right) + \left(\frac{1}{h_{out,2}}\right)\right]^{-1} \tag{4}$$

$$U_4 = \left[2\left(\frac{b_{ms}}{k_{ms}}\right) + \left(\frac{b_I}{k_I}\right) + \left(\frac{1}{h_{out,4}}\right)\right]^{-1} \tag{5}$$

The conductivity of the metal sheets and the insulation layer were considered constant and equal for the top and bottom walls. The outside convection heat transfer coefficients, $h_{out,2}$ and $h_{out,4}$, were based on a well-known literature correlation for horizontal plates subjected to natural convection [18]. The temperatures used in the correlations were based on the experimental mean temperatures of the external metal sheets, which covers the top and bottom surfaces. The mean value for the heat transfer coefficients were found to be equal to 1.7 and 1.0 [W/m^2 K] for the external sheets that cover the top and bottom surfaces of the prototype respectively.

The convective heat transfer coefficients h_1, h_2, and h_4, presented in Eqs. (1)–(3), were determined according to the following expression, as described in [19]:

$$\overline{Nu}_L = 0.037 Re_L^{4/5} Pr^{1/3}, \quad Pr \geqslant 0.5 \tag{6}$$

where Re_L is the Reynolds number, and Pr is the Prandtl number. This correlation is valid for a mixed laminar and turbulent flow over a flat plate. The mixed flow regime is a reasonable assumption, since four small ventilators were used close to the bottom and the top walls to promote a turbulent internal flow in the experimental setup.

The theoretical prescribed temperature of surfaces 1 and 3 was obtained by setting T_1 and T_3 equal to the average temperature readings of the four condensers of the thermosyphons used in the experimental prototype. Based on these experimental data, a theoretical expression for the temperatures T_1 and T_3 was adjusted as a function of time. Such function ruled the heating process on the theoretical model. The agreement of the adjusted function and the experimental data can be considered good, with deviations no larger than ±2 °C.

At this point, the net radiation heat exchange needs to be addressed to Eqs. (2) and (3), and the energy absorbed by any internal surface has to be determined. For this analysis, the method described in [20] was applied. Let us consider a coefficient named G_{jk}, which represents the fraction of radiative energy emitted from surface A_j that reaches and is absorbed by surface A_k. The G_{jk} coefficient cannot be zero, since even for a convex surface, some radiative energy will be returned to itself by reflection from other surfaces. Considering $A_j\varepsilon_j\sigma T_j^4 G_{jk}$ as the fraction of energy emitted by the surface A_j, which is absorbed by A_k, the liquid heat flux for the surface A_k is

$$\begin{aligned} Q_k = {} & A_k\varepsilon_k\sigma T_k^4 - (A_1\varepsilon_1\sigma T_1^4 G_{1k} + A_2\varepsilon_2\sigma T_2^4 G_{2k} + \cdots + A_j\varepsilon_j\sigma T_j^4 G_{jk} + \cdots + A_k\varepsilon_k\sigma T_k^4 G_{kk} + \cdots \\ & + A_N\varepsilon_N\sigma T_N^4 G_{Nk}) \end{aligned} \tag{7}$$

On the other hand, knowing that the total energy emitted from A_j is $A_j\varepsilon_j\sigma T_j^4$, we can say that the portion that reaches A_k directly and is absorbed is $A_j\varepsilon_j\sigma T_j^4 F_{j-k}\varepsilon_k$, where F_{j-k} is the view factor between the surfaces j and k, and $\varepsilon_k = \alpha_k$ for a gray surface. It is important to note that all other radiative energy emitted from A_j and arriving at A_k, will undergo to at least one reflection. Generalizing, we can evaluate the radiation from A_j that arrives to any typical surface such as A_N, and it is reflected as $A_j\varepsilon_j\sigma T_j^4 F_{j-N}\rho_N$, where ρ_N is the reflectivity of the surface N. Only the G_{Nk} heat

fraction reaches A_k and is absorbed. Therefore, all the energy fractions absorbed at A_k that is originated from A_j is

$$Q_{kj} = \underbrace{A_j\varepsilon_j\sigma T_j^4 F_{j-k}\varepsilon_k}_{\text{Energy absorbed directly}} + \underbrace{(A_j\varepsilon_j\sigma T_j^4 F_{j-1}\rho_1 G_{1k} + A_j\varepsilon_j\sigma T_j^4 F_{j-2}\rho_2 G_{2k} + \cdots + A_j\varepsilon_j\sigma T_j^4 F_{j-k}\rho_k G_{kk} + A_j\varepsilon_j\sigma T_j^4 F_{j-N}\rho_N G_{Nk})}_{\text{Energy absorbed indirectly}} \tag{8}$$

The G_{ij} coefficient can be determined by the expression resulting from the sum of the total energy emitted by A_j and Eq. (8), which results in

$$G_{jk} = F_{j-k}\varepsilon_k + F_{j-1}\rho_1 G_{1k} + F_{j-2}\rho_2 G_{2k} + \cdots + F_{j-k}\rho_k G_{kk} + \cdots + F_{j-N}\rho_N G_{Nk} \tag{9}$$

If Eq. (9) is applied to all k surfaces of the enclosure, a system of equations, which has to be solved for $G_{1k}, G_{2k}, \ldots G_{Nk}$, will be formed. This system can be represented by the matricial equation, $[G_{jk}] = [m^{-1}] \times [f]$. For the present case, m and f are

$$m = \begin{bmatrix} (1 - F_{1\text{-}1}\rho_1) & F_{1\text{-}2}\rho_2 & F_{1\text{-}3}\rho_3 & F_{1\text{-}4}\rho_4 \\ F_{2\text{-}1}\rho_1 & (1 - F_{2\text{-}2}\rho_2) & F_{2\text{-}3}\rho_3 & F_{2\text{-}4}\rho_4 \\ F_{3\text{-}1}\rho_1 & F_{3\text{-}2}\rho_2 & (1 - F_{3\text{-}3}\rho_3) & F_{3\text{-}4}\rho_4 \\ F_{4\text{-}1}\rho_1 & F_{4\text{-}2}\rho_2 & F_{4\text{-}3}\rho_3 & (1 - F_{4\text{-}4}\rho_4) \end{bmatrix} \tag{10}$$

$$f = \begin{bmatrix} F_{1\text{-}1}\varepsilon_1 & F_{1\text{-}2}\varepsilon_2 & F_{1\text{-}3}\varepsilon_3 & F_{1\text{-}4}\varepsilon_4 \\ F_{2\text{-}1}\varepsilon_1 & F_{2\text{-}2}\varepsilon_2 & F_{2\text{-}3}\varepsilon_3 & F_{2\text{-}4}\varepsilon_4 \\ F_{3\text{-}1}\varepsilon_1 & F_{3\text{-}2}\varepsilon_2 & F_{3\text{-}3}\varepsilon_3 & F_{3\text{-}4}\varepsilon_4 \\ F_{4\text{-}1}\varepsilon_1 & F_{4\text{-}2}\varepsilon_2 & F_{4\text{-}3}\varepsilon_3 & F_{4\text{-}4}\varepsilon_4 \end{bmatrix} \tag{11}$$

The explicit finite difference approximation was used for the time derivative of the temperature of the air and the surfaces 2 and 4 that appear in Eqs. (1)–(3). The discretized resulting non-linear system was solved numerically using the mathematical software MAPLE. The time interval between two consecutive iterations was one second, $\Delta t = 1$ s. The processing time was around 45 min using a computer with 1 GHz processor and 512 Mb RAM. Table 1 contains the values of the thermophysical properties used in the computation of the equations above.

Table 1
Thermophysical properties and parameters used in the theoretical model

Average specific heat of air ($c_{p,\text{air}}$)	1000 J kg^{-1} K^{-1}
Average specific heat of the metals sheets ($c_{p,1\text{-}4}$)	440 J kg^{-1} K^{-1}
Density of dry air (ρ_{air})	1 kg m^{-3}
Density of metal sheets ($\rho_{1\text{-}4}$)	7850 kg m^{-3}
Emissivity of metal sheets ($\varepsilon_{1\text{-}4}$)	0.2
Global heat transfer coefficient—top surface (U_2)	1.7 W m^{-2} K^{-1}
Global heat transfer coefficient—bottom surface (U_4)	1 W m^{-2} K^{-1}
Metal sheet thermal conductivity	45 W m^{-1} K^{-1}
Dry air thermal conductivity	0.035 W m^{-1} K^{-1}
Stefan–Boltzmann constant (σ)	5.7×10^{-8} W m^2 K^{-4}
Metal sheet thickness (b_{ms})	0.002 m
Insulation thickness (b_{I})	0.0254 m
Outside environment surface (T_{out})	25 °C

3. Experimental apparatus

As a second part of this study, an experimental prototype was build at Federal University of Santa Catarina aiming to determine the real applicability of two-phase thermosyphons as a heat transfer devices between the combustion and cooking chambers. Instead of using a real size prototype, an internal section (i.e., a "slice") of a commercial oven was experimentally simulated. The prototype has a cross section area of 1270 mm (height) × 800 mm (width) including the insulation, which was made of a special fiber for high temperatures, and was 25 mm thick on the top and bottom surfaces and 50 mm thick in each vertical wall. The insulation configuration is shown in detail in Fig. 2.

Stainless steel/water thermosyphons were installed vertically close to two lateral walls of this section. To improve the heat exchange, stainless steel fins are coupled to the thermosyphons as shown in Fig. 3. The stainless steel material was selected due to its strength and durability when submitted to internal high pressures. Also, the stainless steel is a convenient material for the food industry. Water was chosen as the working fluid because it is safe and cheap, presenting a good behavior in terms of heat transfer capacity for the temperature working range around 300 °C [21,22]. The thermosyphons used in the prototype present an unusual geometry as described in [17]. According to Mantelli et al. [17], such a configuration of the thermosyphon presented a good thermal behavior with a temperature difference between the condenser and evaporator less than 20 °C.

The thermosyphons have 1220 mm of total length, where 1000 mm corresponds to the condenser, 200 mm to the evaporator and 20 mm to the adiabatic section. Their external diameters

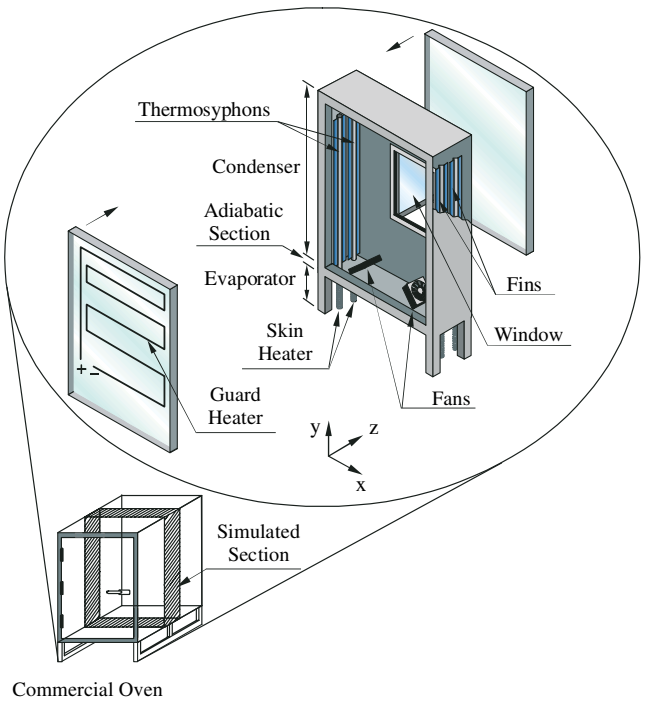

Fig. 3. Experimental setup sketch.

are 19.05 mm and the filling ratio is 60% of the evaporator volume [22–24]. The power was applied manually and varied between 50 and 200 W per evaporator, in 50 W steps of 30 min each. The heat was delivered to the evaporator by an electrical skin heater built in order to mimic a combustion chamber. The skin heater was made of a flat wire electrical resistance sandwiched by two layers of an appropriated electrical insulator. The experimental temperature limit was selected equal to 260 °C at any point in the evaporator. At this temperature level the skin heater electrical insulation starts to degrade, risking the whole apparatus. The four fans installed inside the prototype provided the mixed convection regime inside the cooking chamber. Two of them were installed close to the bottom surface, and the other two were fixed closed to the top surface in order to prevent any excessive thermal stratification. These fans are the exact same model used to cool down computer; hence, they have low power.

Since we are simulating just a "slice" of a real oven, electric guards heaters were installed on the exterior side of the frontal and back walls to maintain the front and back walls adiabatic. The guard heaters were fabricated with the same resistive flat wire used as a skin heater on the thermosyphons' evaporators. Figure 3 shows that the distance between the flat wires is smaller on the top of the front and back walls. This was required due to a slightly experimental temperature gradient found on y-direction.

Approximately 30 thermocouples type K where installed on the prototype for the temperature measurement of the heated air and internal walls. About five thermocouples were installed equidistantly on each thermosyphon, two on each the evaporator and three on each condenser. These thermocouples were connected to a Hewlett Packard-34970A acquisition data system, which was connected to a computer. The readings were made every one second. Using these readings, the prototype temperatures were determined and compared with the theoretical model described in Section 2.

Figure 4 shows the comparison between the mean internal and external temperatures of the front wall. We can see that the temperature levels are very similar, showing that negligible heat is being transferred throughout the wall. In other words, the guard heater proved to be efficient. A similar curve can be observed for the rear vertical wall, but it will not be presented here. The disagreement found around 140 °C is due to a limitation of the guard heater power supply.

The electric power applied to each thermosyphon is shown in Fig. 5. In the same figure the liquid power applied, which is defined as the total applied heat minus the heat losses, is also shown. The heat losses always represent less than 8% of the total electric power. They were determined by accounting the temperature difference between the evaporators' external thermal insulation surface and the environment.

4. Experimental uncertainty

The applied power in the evaporators and in the guard heater were calculated from the expression, $P = V \times I$, which is also used to determine the power uncertainty. The uncertainty of the independent variables $I = 10 \pm 0.01$ and $V = 100 \pm 0.1$ was propagated to the power using the method described in [25], presenting a value equal to 1000 ± 1.414 W.

The thermocouples were calibrated through the whole range of temperature under consideration, starting at the water melting temperature 0 °C at one atmosphere to the upper limit

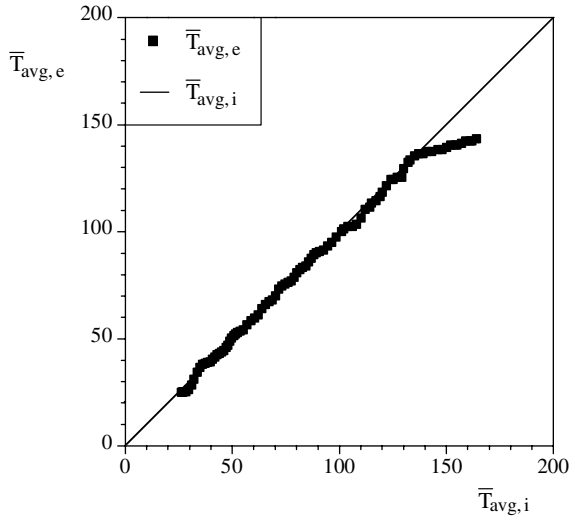

Fig. 4. Comparison of experimental internal and external front wall averaged temperature (guard heater efficiency).

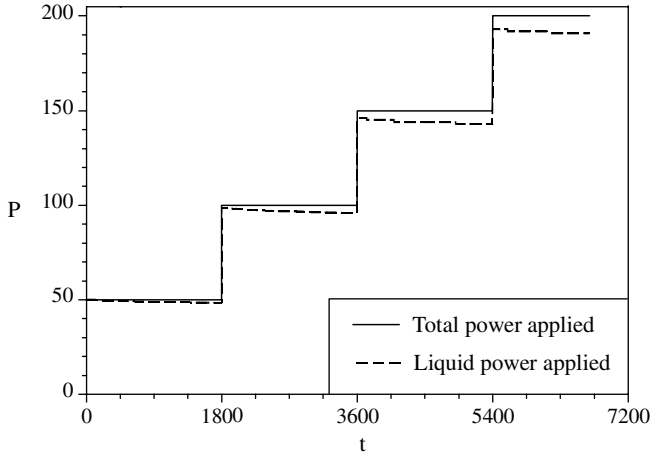

Fig. 5. Experimental electric power applied to each evaporator.

temperature, which always happens to occur in one of the four evaporators ($T_{max} \cong 260$ °C). The calibration error found was much lower than the error indicated by the manufacturer, ±2.2 °C. Conservatively, ±2.2 °C reading error was adopted to all temperature measurements.

5. Results and discussion

In this section, we will discuss the results concerning the thermal behavior of thermosyphons inside our prototype. Figure 6 shows the variation of the averaged temperature difference between

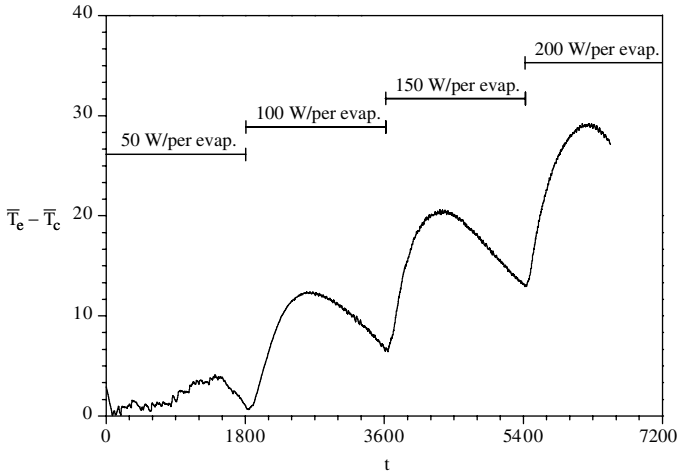

Fig. 6. Averaged temperature difference between the evaporator and condenser.

the evaporator and condenser. An oscillatory behavior can be seen when $t < 1800$ (i.e., 50 W/per evaporator). The explanation for that resides on the so-called Geyser effect [17]: at low heat input, the thermosyphons work under a regime where large random bubbles of size of the same order of the tube diameter, grow on the evaporator carrying over them large amount of liquid working fluid towards the condenser. Those bubbles collapse as soon as they reach the condenser section. At this level of heat input, the thermosyphons do not present a good thermal performance in terms of uniform temperature distribution on the condensers. However at higher levels of heat input, i.e., for $1800 < t < 3600$ ($P = 100$ W), $3600 < t < 5400$ ($P = 150$ W), and finally for $5400 < t < 7200$ ($P = 200$ W), the averaged difference of temperatures between the evaporator and condenser presents a "smoother" shape. For $t \geqslant 1800$, each time period of constant power input presents one maximum and two minimums values of the $\overline{T}_e - \overline{T}_c$ parameter. The maximum is located at approximately half of each time period. The two minimums occur at the beginning and at the end of each time period. This temperature difference physical behavior shows that there is a "time delay" required to warm up the evaporator and consequently to transfer the energy to the cooking chamber while, in this mean time, the evaporator's temperature raises faster. By defining the thermosyphon global conductance as

$$C = \frac{Q}{(\overline{T}_e - \overline{T}_c)H_e} \tag{12}$$

where H_e is the evaporator height, it is easy to see that the larger the difference $\overline{T}_e - \overline{T}_c$, the worse the thermal performance of the thermosyphon for a fixed heat input. Therefore, observing Fig. 6, we can see that during around half of the heating time, for each power time step, the thermal performance of the thermosyphon decreases to a minimum value located close to the mean time step. After that, the performance increases again. As $\overline{T}_e - \overline{T}_c$ did not reach a constant value in any of the power input time steps, we can say that the steady-state regime was not achieved in the present experiment. Furthermore, in Fig. 6, we can conclude that the thermosyphons' evaporators should be exposed to a smooth power raising input, until the temperature required inside the

cooking chamber is reached. This kind of heating process will avoid the temperature peaks shown in Fig. 6, and consequently maximize the thermosyphons' global conductance. It should be noted that the experimental run stopped at $t \cong 6300$ s, because as mentioned earlier in Section 3, the maximum allowed temperature in any point of any one of the four evaporators is 260 °C. At this point the electrical insulation of the skin heaters starts to degrade.

Figure 7 shows the experimental isothermal lines inside the prototype at the end of the test (i.e., $t \cong 6300$ s). It can be observed that in spite of the temperature gradient in x-direction between the two vertical walls (i.e., $x = 0$ and $x = 0.7$) and the center is around 50 °C, no overheated spot is found, and the temperature distribution on the vertical wall is practically uniform. The same happens in the vertical plane of symmetry ($x = 0.35$), where the air temperature is about 160 °C all over the prototype, showing just a little of stratification in the upper side, which reaches less than 190 °C.

Figure 8 shows a comparison between the mean temperature of the air inside the prototype and a theoretical curve based on the characteristic velocity $v = 0.5$ ms^{-1}. This comparison shows that the theoretical model over estimate the mean temperature obtained from theoretical curve in about 15 °C for $t \cong 5400$ s. This difference can be attributed to the convection heat transfer coefficients associated with each internal surface. The values used in the model for these coefficients were obtained from the literature [19] for mixed turbulent convection over flat plates in open environments. Furthermore, the data was obtained from a rectangular cavity where the natural air circulation is enhanced by four small fans, which were not able to create the same flow conditions assumed in the model. Besides the simplicity of the theoretical model, its robustness

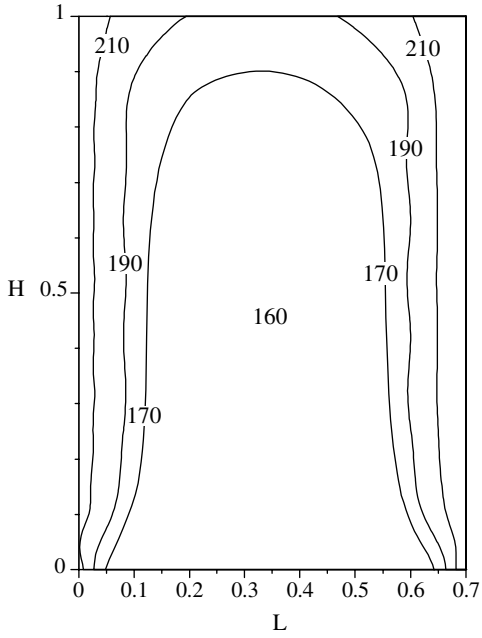

Fig. 7. Experimental temperature distribution inside the prototype—isothermal lines.

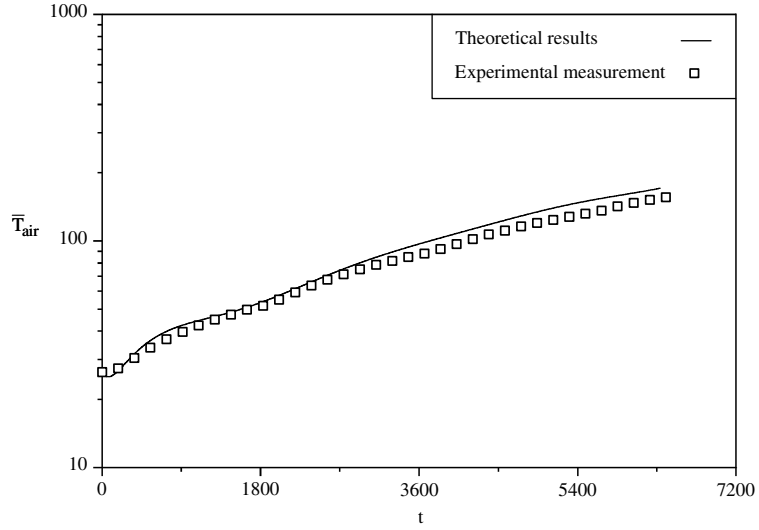

Fig. 8. Enclosed air temperature variation—experimental and theoretical comparison.

should be recognized due to the agreement between the experimental and theoretical curves, which can be considered satisfactory.

The same analysis was performed for the two other transient temperatures obtained from the theoretical model, T_2 and T_4, while T_1 and T_3 were input parameters obtained from the adjustment between an analytical expression and the experimental data. Figure 9 shows the comparison between the experimental temperature of the top surface T_2, and the theoretical model for the same characteristic velocity used in Fig. 8. Figure 10 shows a similar curve for the bottom surface.

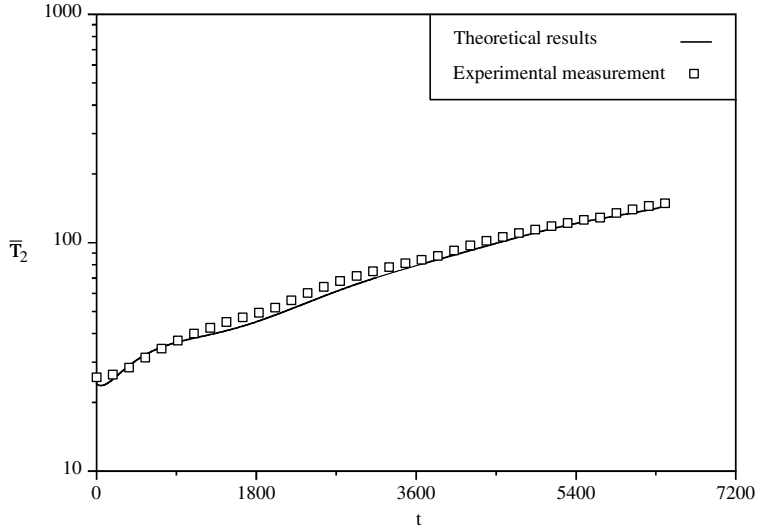

Fig. 9. Top surface temperature variation ($\overline{T}_2$)—experimental and theoretical comparison.

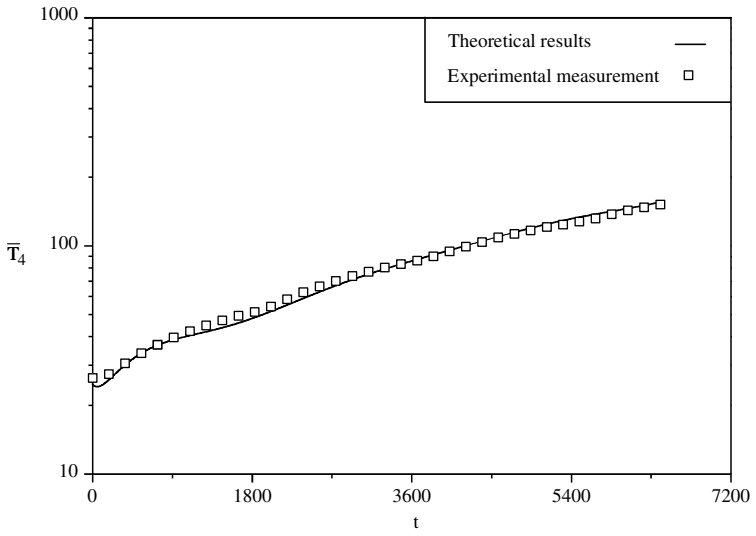

Fig. 10. Bottom surface temperature variation ($\overline{T}_4$)—experimental and theoretical comparison.

It should be noted that the characteristic velocities were not measured. Several theoretical values were used in the model with the objective of getting a curve that presents a good comparison with the data. This good comparison obtained was always obtained for low velocities (i.e., $v \leqslant 2\ \mathrm{ms}^{-1}$) showing that the convection heat transfer, which is proportional to the air velocity flowing over a surface inside the chamber, does not play the major role. The greatest part of the heat is transferred by radiation. It should be noted that Figs. 9 and 10 show a better agreement between the theoretical results and experimental measurements than Fig. 8. This happens because the temperature of the air inside the chamber is completely heated by convection. On the other hand, the internal walls receive energy by radiation, which was precisely determined by the theoretical model.

To better illustrate this point, Fig. 11 shows the dimensionless contribution of the radiative heat flux (i.e., $\hat{q}_{\mathrm{rad}} = q_{\mathrm{rad}}/q_{\mathrm{Total}}$), and convective heat flux (i.e., $\hat{q}_{\mathrm{conv}} = q_{\mathrm{conv}}/q_{\mathrm{Total}}$), where $q_{\mathrm{Total}} = q_{\mathrm{conv}} + q_{\mathrm{rad}}$. In other words, the vertical axis represents the convective or the radiative fraction of energy heat flux leaving the thermosyphons' condenser. The horizontal axis is the dimensionless time $\hat{t} = \alpha t/H^2$, where α is defined as the air thermal diffusivity, t is the time and H is the characteristic surface length (i.e., condenser length). Several curves were plotted for different wall emissivities. It can be observed that for the initial time $\hat{t} = 0$, all the curves are close together and for every instant with a fixed wall emissivity, the sum of the dimensionless radiative and convective heat flux is equal to 1. As the time goes by, the walls and the air are being heated up by convection at different rates. For $\varepsilon = 0.9$, the difference between the radiation and convection is more evident due to the high amount of energy that the walls are able to absorb by radiation. In this case, most of the energy that reaches the internal walls is absorbed by radiation and transferred by convection to the enclosed air. The higher the internal wall emissivity, the faster the thermal response of the internal walls and consequently the smaller the convection heat transfer, which is strongly related with the temperature of the air inside. For $\varepsilon = 0.9$, the radiative heat flux represents about

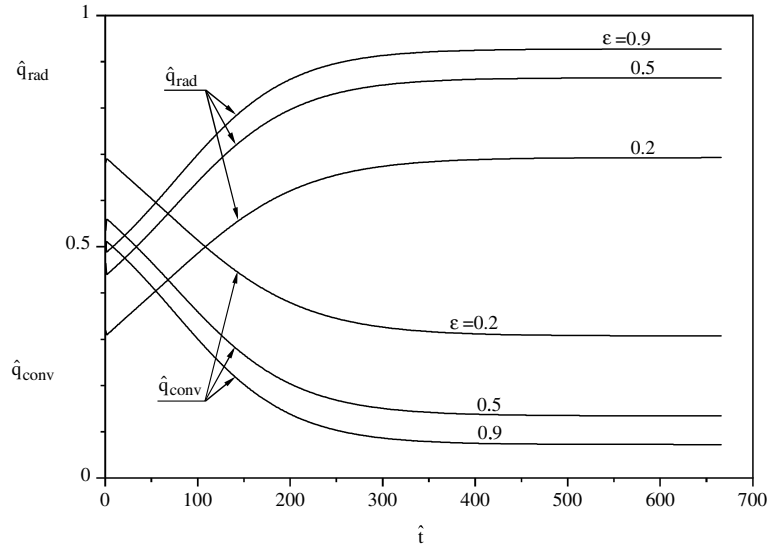

Fig. 11. Theoretical convective and radiative dimensionless heat flux.

90% of the total energy exchanged within the enclosure, and the convective heat flux represents about 10%. This analysis implies that the radiation heat transfer primarily dominates the heat transfer in a cooking chamber. Assuming the internal walls with $\varepsilon = 0.2$ (i.e., which is approximately the order of magnitude of polish steel commonly used inside ovens), Fig. 11 shows that most of the energy emitted by radiation from the vertical walls is reflected within the internal walls, delaying the walls and the inside air heating up process. For $\varepsilon = 0.2$, the radiation represents 65% of the total energy that enters within the enclosure. For the intermediate value of emissivity, $\varepsilon = 0.5$, the radiation suppresses the convection heat flux by a factor of 4. Similar curves could be plotted for the other surfaces, but they will not be presented here.

These are very interesting results that can lead to important conclusions with respect to the thermal applicability of thermosyphons in cooking chambers, specially if we consider a real situation where any unbaked product is placed inside the oven/furnace. By associating the experimental temperature distribution shown in Fig. 7 with the heat transfer modes shown in Fig. 11, it is reasonable to conclude that the thermosyphon are consistently eligible for such application. The reason for that stems from the fact that any unbaked product will bake uniformly when exposed to such an approximately uniform temperature distribution environment (Fig. 7), and, at the same time, to a uniform radiation network at low temperature (i.e., $T_{\text{hot wall}} \cong T_{\text{air}}$) provided by the surrounding hot walls (i.e., thermosyphons' condensers).

6. Conclusions

In the present work we designed and built an experimental prototype to investigate the applicability of thermosyphons as heat transfer devices in ovens or furnaces. The experimental

measurements were used to validate the theoretical model, which, in turn, was used to predict the magnitude of the convective and radiative heat transfer modes inside the cooking chamber.

The experimental distribution of temperature inside the prototype was shown to be highly uniform due to the large area of the condenser responsible for the heating of the cooking chamber. The radiative heat flux still is the larger fraction of incoming energy inside the cooking chamber and no over-heated spots were found. Therefore, the incidence of radiative energy over any product placed in the cooking chamber will be highly uniform, avoiding over/under cooked products.

It was also shown that the imposed heat to the thermosyphons (i.e., electric skin heater or burner of any fuel for example) should not be abrupt in order to avoid any kind of over-heating on the evaporator, which will decrease the thermosyphon global conductivity drastically.

The model also showed that the internal temperatures of the prototype can be determined theoretically with a good precision. Based on that, we can use the results obtained in the present work to estimate the energy savings associated with the application of thermosyphons technology in bakery ovens in comparison with the usual heating methods used in the market.

Acknowledgements

The authors would like to acknowledge Mr. Ricardo A. Penteado and Mr. Lindomeilo J. de Souza for their support during the construction of the experimental prototype, and the financial support from CNPq-Desenvolvimento Científico e Tecnológico (Brazil), CAPES-Coordenação de Aperfeiçoamento de Pessoal de Nível Superior (Brazil) and PETROBRAS/CENPES.

References

[1] A.R. Lukitobudi, A. Akbarzadeh, P.W. Johnson, P. Henry, Design, construction and testing of a thermosyphons heat exchange for medium temperature heat recovery in bakeries, Heat Recovery Systems CHP 15 (1995) 481–491.
[2] J.C. Bratis, J.L. Novotny, Radiation–convection interaction in the boundary layer regime of an enclosure, Int. J. Heat Mass Transfer 17 (1974) 23–36.
[3] D.W. Larson, R. Viskanta, Transient combined laminar free convection and radiation in a rectangular enclosure, J. Fluid Mech. 78 (1976) 65–85.
[4] L.C. Chang, K.T. Yang, J.R. Lloyd, Radiation–natural convection interactions in two-dimensional complex enclosures, J. Heat Transfer 105 (1983) 89–95.
[5] Z.Y. Zhong, K.T. Yang, J.R. Lloyd, Variable property natural convection in titled enclosures with thermal radiation, Numer. Meth. Heat Transfer 3 (1985) 195–214.
[6] A. Yucel, S. Acharya, M.L. Williams, Natural-convection and radiation in a square enclosure, Numer. Heat Transfer A 15 (1989) 261–278.
[7] M. Akiyama, Q.P. Chong, Numerical analysis of natural convection with surface radiation in a square enclosure, Numer. Heat Transfer A 32 (1997) 419–433.
[8] N. Ramesh, S.P. Venkateshan, Effect of surface radiation on natural convection in a square enclosure, J. Thermophys. 13 (1999) 299–301.
[9] N. Li, Z.X. Li, Relative importance of natural convection and surface radiation in a square enclosure, Int. J. Nonlinear Sci. Numer. Simulat. 3 (2002) 613–616.
[10] M.G. Carvalho, N. Martins, Heat and mass transfer in an electrically heated natural convection baking oven, First European Thermal-Sciences and Third UK National Heat Transfer Conference, UK, vol. 129, 1992, pp. 699–708.

[11] F.D. Haynes, J.P. Zarling, G.E. Gooch, Performance of a thermosyphons with a 37 meter-longer, horizontal evaporator, Cold Regions Sci. Technol. (1992) 261–269.
[12] S.S. Nam, S.B. Choi, J.H. Kim, H.Y. Kwak, Transient characteristics of a two-phase thermosyphon loop for multichip module, ETRI J. 20 (1998) 284–300.
[13] R. Stegmann, Thermosyphon oil coolers, ASHRAE J. 43 (2001) 59–60.
[14] H.M.S. Hussein, Transient investigation of a two phase closed thermosyphon flat plate solar water heater, Energy Convers. Mgmt. 43 (2002) 2479–2492.
[15] A. Faghri, Heat Pipe Science and Technology, Taylor and Francis, Washington, 1995.
[16] P.D. Dunn, D.A. Reay, Heat Pipes, fourth ed., Pergamon, 1994.
[17] M.B.H. Mantelli, S. Colle, D.U.C. Moraes, R.D.M. Carvalho, Study of Two-Phase Thermosyphons for Bakeries Oven Applications, 33rd National Heat Transfer Conference, Albuquerque, New Mexico, USA, 1999.
[18] A. Bejan, Heat Transfer, John Wiley and Sons, New York, 1993.
[19] A. Bejan, Convection Heat Transfer, second ed., John Wiley and Sons, New York, 1995.
[20] R. Siegel, J.R. Howell, Thermal Radiation Heat Transfer, Taylor and Francis, Washington, D.C., 1992.
[21] O. Brost, Closed Two-Phase Thermosyphons, Class Notes, IKE, University of Stuttgart, Germany, 1996.
[22] G.P. Peterson, An Introduction to Heat Pipes, John Wiley and Sons, New York, 1994.
[23] M. Groll, S. Rösler, Operation principles and performance of heat pipes and closed two-phase thermosyphons, J. Non-Equilib. Thermodyn. 17 (1992) 91–151.
[24] F. Kaminaga, H. Hashimoto, M.D.C. Feroz, K. Goto, K. Matsumura, Heat transfer characteristics of evaporation and condensation in two-phase closed thermosyphons, Eighth IHPC, Beijing, China, 1992.
[25] J.P. Holman, Experimental Methods for Engineering, sixth ed., McGraw-Hill, Singapore, 1994.